Defense Technical Information Center
Compilation Part Notice

ADP012521

TITLE: Trapped Particle Asymmetry Modes in Non-Neutral Plasmas

DISTRIBUTION: Approved for public release, distribution unlimited

This paper is part of the following report:

TITLE: Non-Neutral Plasma Physics 4. Workshop on Non-Neutral Plasmas [2001] Held in San Diego, California on 30 July-2 August 2001

To order the complete compilation report, use: ADA404831

The component part is provided here to allow users access to individually authored sections of proceedings, annals, symposia, etc. However, the component should be considered within the context of the overall compilation report and not as a stand-alone technical report.

The following component part numbers comprise the compilation report:
ADP012489 thru ADP012577

Trapped Particle Asymmetry Modes in Non-Neutral Plasmas

Andrey A. Kabantsev, C. Fred Driscoll, Terry J. Hilsabeck,
Thomas M. O'Neil, and Jonathan H. Yu

Physics Department, University of California at San Diego, La Jolla CA 92093-0319 USA

Abstract.
  Novel trapped particle asymmetry modes propagate on cylindrical electron columns when axial variations in the wall voltage cause particle trapping. These modes consist of $\mathbf{E} \times \mathbf{B}$ drifts of edge-trapped particles, partially shielded by axial flows of interior untrapped particles. A simple theory model agrees well with the observed frequencies and eigenfunctions; but the strong mode damping is as yet unexplained. These modes may be important in coupling trap asymmetries to particle motions and low frequency $\mathbf{E} \times \mathbf{B}$ drift modes.

INTRODUCTION

Single species plasmas confined in cylindrical traps with static electric and magnetic fields are utilized in research ranging from basic plasma and fluid dynamics to spectroscopic frequency standards to anti-matter containment [1]. The plasma confinement times can be hours or days, generally limited by azimuthal asymmetries in the trapping fields which couple angular momentum into the rotating plasma [2]. This coupling can be enhanced by mode resonances [3], and plasma modes occur on frequency scales ranging from the (high) cyclotron frequency Ω_c, to the plasma frequency ω_p, to the (low) $\mathbf{E} \times \mathbf{B}$ drift frequency ω_E. However, the well-studied "diocotron" drift modes have axial wavenumber $k_z \simeq 0$, and so do not readily couple the plasma electrostatic energy into particle kinetic energy.

  Here, we describe novel "trapped particle asymmetry" modes which propagate azimuthally at low $\mathbf{E} \times \mathbf{B}$ drift frequencies, but which have $k_z \neq 0$ and thus couple to particle kinetics. These modes exist when axial variations in the wall potential cause the equilibrium plasma to have axially trapped particles. Experimentally, we generate the trapped particles by applying a "squeeze" voltage to a central cylindrical electrode; but smaller trapping potentials are caused by wall irregularities, and are probably endemic to these traps.

  These asymmetry modes can have azimuthal mode number $m = 1, 2, ...$, but we focus on $m = 1$ here. Dynamically, the modes are an $\mathbf{E} \times \mathbf{B}$ drift motion of the edge-trapped particles, with axial flows of interior untrapped particles giving partial Debye shielding. A simple theory model with these characteristics shows close correspondence with the measured frequencies and radial eigenfunctions of the modes. The modes are observed to be strongly damped, but this damping is not yet understood. These modes are particularly simple cylindrical analogues to the trapped drift modes which can contribute
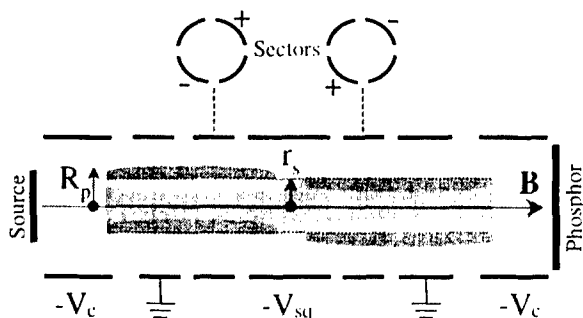
FIGURE 1. Schematic of the cylindrical trap with "squeezed" electron column and applied sector voltages.

to anomalous plasma transport in tokamak-like and toroidal multipole configurations of neutral plasmas [4, 5].

EXPERIMENTAL SETUP

The cylindrical confinement geometry and a schematic of the mode are shown in Fig. 1. A nominally cylindrical column of electrons from a hot tungsten source is confined radially by a uniform magnetic field $B = 4$ kG and confined axially by negative voltages $-V_c = -100$ V on end cylinders. Typical electron columns have a central density $n_0 \approx 1.5 \times 10^7$ cm^{-3} over a length $L_p \approx 50$ cm, with a column radius of $R_p \approx 1.2$ cm inside a wall radius $R_w = 3.5$ cm. The z-averaged electron density $n(r, \theta, t)$ can be (destructively) measured at any time by dumping the electrons axially onto a phosphor screen imaged by a CCD camera [6].

The individual electrons have a thermal energy $T \approx 1$ eV, giving an axial bounce frequency $f_b \equiv \bar{v}/2L_p \approx 0.5$ MHz and a Debye shielding length $\lambda_D \equiv (T/4\pi e^2 n)^{1/2} \approx 0.2$ cm. The unneutralized electron charge results in a central potential $\phi_0 \approx -30$ V, and the radial electric field causes the column to $\mathbf{E} \times \mathbf{B}$ drift rotate at a rate $f_E(r) \equiv cE(r)/2\pi rB \lesssim 50$ kHz. Figure 2 shows typical radial profiles of density and rotation for a θ-symmetric column.

When a negative "squeeze" voltage $-V_{sq}$ is applied to a central cylinder, electrons are excluded from the column periphery under the squeeze ring, and those electrons located at radii at $r > r_s$ are trapped axially in one end or the other. For small V_{sq}, a fraction $\varepsilon_{tr} \approx V_{sq}/\phi_0$ of all the electrons are trapped axially.

Linear $\mathbf{E} \times \mathbf{B}$ drift modes with azimuthal mode numbers $m = 1, 2, \ldots$ propagate on this trapped particle equilibrium. The ubiquitous $m = 1$ center-of-mass "diocotron" mode is essentially uniform in z (i.e. $k_z \approx 0$), and is nominally unaffected by small V_{sq}. In contrast, the $m = 1$ "trapped particle asymmetry" mode described here has odd parity in z: the perturbations are essentially uniform within each end, but of *opposite sign* on either side of the squeeze, as shown schematically in Fig. 1. Moreover, the perturbations
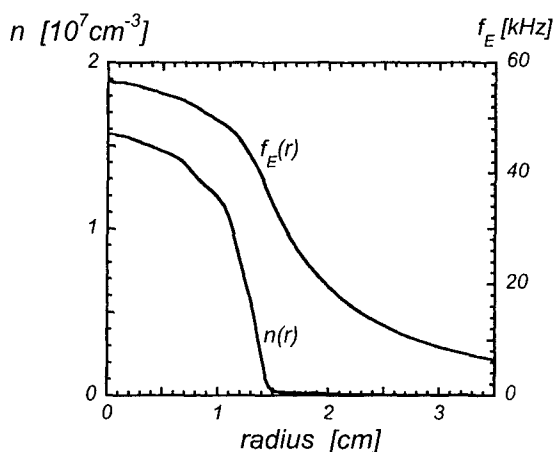
FIGURE 2. Radial profiles of density $n(r)$, and $\mathbf{E} \times \mathbf{B}$ rotation frequency $f_E(r)$.

in the trapped particles at $r > r_s$ are partially "shielded" by perturbations of opposite sign in the untrapped particles at $r < r_s$; and these untrapped particles slosh from end to end in response to the $\mathbf{E} \times \mathbf{B}$ drift evolution of the trapped particles.

Experimentally, these odd-z-parity $m = 1$ asymmetry modes can be excited with $+$ and $-$ voltages applied to opposing wall sectors, with the voltages oppositely phased at the two ends. Any single wall sector can be used as a receiver, or sectors can be used in combination to verify or utilize the θ- and z-symmetries of the modes.

EXPERIMENTAL RESULTS

Figure 3 shows the measured frequencies f_a and f_d as the applied squeeze voltage V_{sq} is varied. The asymmetry mode frequency f_a is at or near the edge rotation frequency $f_E(R_p)$ for $V_{sq} \ll \phi_0$. As V_{sq} is increased, the trapping separatrix r_s moves inward, and f_a decreases. For $V_{sq} \gtrsim \phi_0$, the column is cut in half, and the asymmetry mode becomes degenerate with the diocotron mode. With all particles trapped, the asymmetry mode is equivalent to two separate diocotron modes, 180° out of phase. The diocotron frequency f_d increases slightly with V_{sq}, because the effective line density of the column increases as particles are excluded from the squeeze ring. Both f_a and f_d scale as $f \propto B^{-1}$, as expected for $\mathbf{E} \times \mathbf{B}$ drift modes.

Figure 4 shows that the asymmetry mode damping rate γ_a also depends on V_{sq}, decreasing roughly as $\gamma_a \propto (1 - V_{sq}/\phi_0)$ in the regime $V_{sq} \gtrsim \phi_0/10$ where γ_a can be readily measured. Comparing Figs. 3 and 4, we can see that $\gamma_a/f_a \lesssim 1/20$, so the mode is strongly damped except at $V_{sq} \gtrsim \phi_0$. However, we observe essentially no magnetic field dependence to the damping [at fixed V_{sq}/ϕ_0] in the range of 0.39 kG $\leq B \leq$ 10 kG, i.e. $\gamma_a \propto B^0$. (A weak dependence on B arises experimentally because the equilibrium plasma potential ϕ_0 depends weakly on B.) Thus, $\gamma_a/f_a \propto B^1$ and the mode is relatively
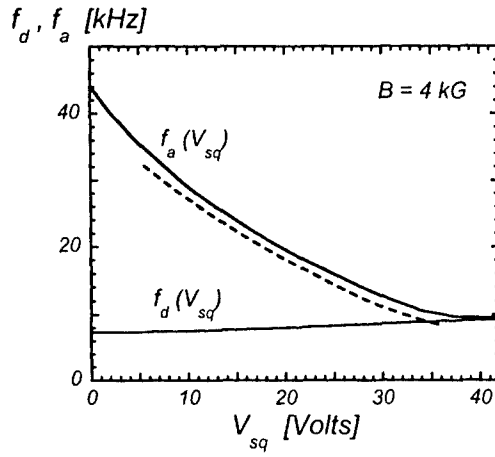
FIGURE 3. Measured frequencies f_a and f_d vs squeeze voltage V_{sq}; f_a calculated from the kinetic model (dashed).
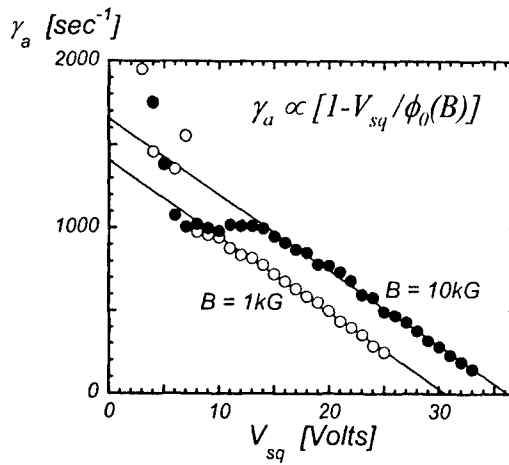

FIGURE 4. Measured decay rate γ_a of the asymmetry mode vs squeeze voltage V_{sq} at two extreme values of the magnetic field. Plasma potential ϕ_0 is less at low magnetic field due to enhanced radial transport of the particles.
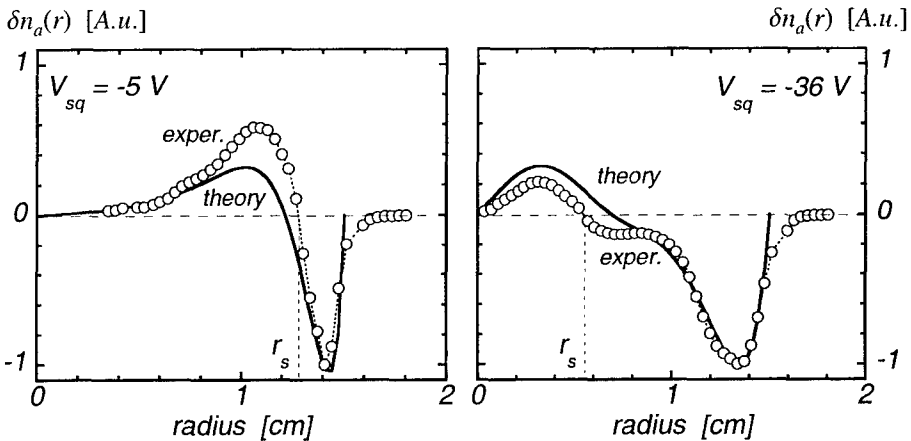
280

FIGURE 5. Measured (circles) and calculated from the kinetic model (solid) asymmetry mode eigenfunctions $\delta n_a(r)$ for $V_{sq} = -5V$ (left) and $V_{sq} = -36V$ (right).

less strongly damped at lower magnetic fields.

As yet, the cause of this damping is not understood, but experimental signatures (like $\gamma_a \propto r_s^1 B^0$) suggest diffusive mixing between the trapped and untrapped populations. Also, for $V_{sq} < \phi_0/10$, there are suggestions that spatial Landau damping (scaling as B^{-1}) may occur, but this damping depends critically on the density profile near R_p.

The density eigenfunctions $\delta n_a(r)$ of the asymmetry mode can be obtained from a time sequence of measurements of the density $n_h(r,\theta,t)$ z-averaged over only *half* the plasma. To dump only half the column, V_{sq} is increased to $-100\,V$ immediately before lowering V_c to dump the plasma onto the phosphor screen. The $m=1$ perturbations in $n_h(r,\theta,t)$ are then fit to a sum of 2 modes (asymmetry and diocotron), as

$$\int d\theta\, n_h(r,\theta,t)\, e^{-im\theta} = \sum_{j=a,d} \delta n_j(r)\, e^{i2\pi f_j t - \gamma_j t}.$$

The residual to this fit is small, and the eigenfunctions are obtained with little ambiguity. The real parts of the asymmetry mode eigenfunction δn_a (scaled arbitrarily) obtained for $V_{sq} = -5V$ and $V_{sq} = -36V$ are shown in Fig. 5; with proper choice of θ-origin, the imaginary part of δn_a is essentially zero.

The mode shows a negative perturbation at $r > r_s$ and a positive perturbation for $r < r_s$; and the signs of these perturbations reverse for $z \to -z$ and for $\theta \to \theta + \pi$. The observed position of the zero-crossing at r_s varies with V_{sq}, consistent with the "waistline" radius obtained from (r,z) Poisson solutions for the equilibrium with the measured charge and applied wall potentials.

281

THEORETICAL MODELS

Fluid theory and kinetic theory models further support the interpretation of the asymmetry mode as trapped $\mathbf{E} \times \mathbf{B}$ drifting edge particles which are Debye-shielded by sloshing interior particles. In these models, the applied squeeze voltage is presumed to create a (zero-length) barrier for particles at $r > r_s$, creating two outer regions with axial lengths L_1 and L_2. In contrast, interior particles with $r < r_s$ move freely over length $L_1 + L_2$.

Because the axial bounce frequency is large compared to the $\mathbf{E} \times \mathbf{B}$ rotation frequency and the mode frequency, the bounce-average density perturbation in any one of the three regions, $\overline{\delta n}$, is related to the bounce-average potential perturbation in that region, $\overline{\delta\phi}$, through

$$\overline{\delta n}(r) = \frac{c}{2\pi Br} \frac{\partial n_0}{\partial r} \frac{m\overline{\delta\phi}(r)}{mf_E(r) - f} \,. \tag{1}$$

Within any of the regions, rapid axial streaming yields the adiabatic response

$$\delta n(r,z) = \overline{\delta n}(r) + \frac{en_0}{T}[\,\delta\phi(r,z) - \overline{\delta\phi}(r)\,]\,. \tag{2}$$

This type of response gives rise to Debye shielding, making $\delta\phi(r,z)$ and $\delta n(r,z)$ nearly z-independent except near the plasma ends and the squeeze region. Thus, we approximate $\delta n(r,z) \approx \delta n_j(r)$ and $\delta\phi(r,z) \approx \delta\phi_j(r)$, with $j = 1,2$ representing the left and right sides relative to the barrier. Poisson's equation for the two sides is then

$$
\frac{1}{r}\frac{\partial}{\partial r} r\left(\frac{\partial}{\partial r}\delta\phi_j\right) - \frac{m^2}{r^2}\delta\phi_j
$$
$$
= \begin{cases}
\dfrac{2ec}{Br}\dfrac{\partial n_0}{\partial r}\dfrac{m\delta\phi_j}{mf_E - f} & , r > r_s \\[3mm]
\dfrac{2ec}{Br}\dfrac{\partial n_0}{\partial r}\dfrac{m\delta\phi_b}{mf_E - f} + \dfrac{4\pi e^2 n}{T}(\delta\phi_j - \delta\phi_b) & , r < r_s
\end{cases}
\tag{3}
$$

Here, $\delta\phi_b \equiv (L_1\delta\phi_1 + L_2\delta\phi_2)/(L_1 + L_2)$ is the potential averaged over both sides, and the boundary condition is $\delta\phi_j(R_w) = 0$.

Fortunately, the even and odd axial symmetries of the diocotron and asymmetry modes decouple the equations. For $\delta\phi_1(r) = \delta\phi_2(r) = \delta\phi_b(r)$, both equations reduce to the usual equation for a diocotron mode. For $L_1\delta\phi_1(r) = -L_2\delta\phi_2(r)$, giving $\delta\phi_b(r) = 0$, we obtain an eigenvalue equation for the asymmetry mode potentials.

For a uniform density profile of density n_0 and radius R_p, the eigenfrequency $f \equiv f_a$ is

$$\frac{f_a}{f_E(0)} = m - \frac{(R_w^{2m} - R_p^{2m})(I_{m-1}R_p^{2m} - I_{m+1}r_s^{2m})}{R_p^{2m}(I_{m-1}R_w^{2m} - I_{m+1}r_s^{2m})}\,. \tag{4}$$

Here, $I_{m\pm1} \equiv I_{m\pm1}(r_s/\lambda_D)$ are modified Bessel functions of the first kind. In the limit of $\lambda_D \to 0$, the interior region acts like a conductor, and the exponentially large $I_{m\pm1}$ may be replaced by 1 in Eq. (4). The boundary r_s is determined by radial integration of Poisson's equation with density n_0 out to radius r_s giving $\phi(R_w) = -V_{sq}$. Figure 6
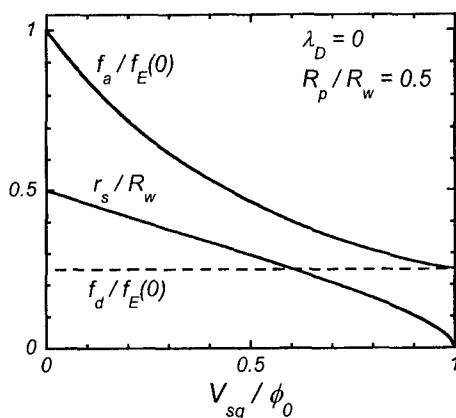
FIGURE 6. Separatrix radius r_s vs V_{sq}/ϕ_0 for uniform density model, giving f_a from Eq. (4) and constant f_d.

shows r_s, f_a, and f_d versus V_{sq} for this uniform density model with $R_p = 0.5R_w$ and $m = 1$. There is an obvious general correspondence between this coarse estimate and the experiment (Fig. 3).

A kinetic analysis allowing for trapped and untrapped particles co-existing at each radius gives a more realistic approximation to the experiments. The squeeze causes a potential barrier of strength $\Delta\phi(r)$, giving a trapped particle density $n_t(r) = n(r)\text{erf}[(e\Delta\phi/T)^{1/2}]$ and an untrapped density $n_u = n - n_t$. The equilibrium Poisson solutions show that $\Delta\phi$ is essentially zero for small radii and that it rises sharply near r_s to a value much larger than T. Thus, the kinetic treatment essentially smoothes the discrete transition model over a radial scale of a few λ_D.

The frequency f_a versus V_{sq} predicted by this kinetic theory using the measured $n(r)$ and the calculated $\Delta\phi(r)$ is given by the dashed curve in Fig. 3, showing close agreement with the measured frequencies. The 10% discrepancy may reflect the non-zero length of the barrier and consequent increase in trapped particle densities.

Similarly, the eigenfunctions $\delta n_a(r)$ obtained from the kinetic analysis show general correspondence with experiments (Fig. 5). The discrepancy for $r \gtrsim 1.5$ cm may be an artifact of the profile truncation applied theoretically.

MAGNETIC TILT, MODE COUPLING AND TRANSPORT

Although the asymmetry modes can propagate in a trap with perfect θ-symmetry, our larger interest is in traps with (inevitable) θ-asymmetries. These asymmetries commonly arise from construction imperfections in the trap walls (especially in the sectored cylinders) or in the magnet. The asymmetries can have arbitrary θ- and z-dependence, but it
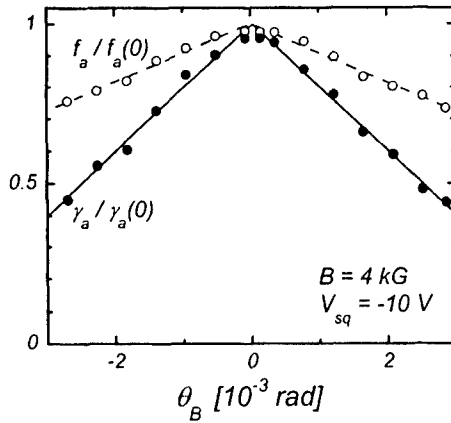
FIGURE 7. Measured frequency f_a and decay rate γ_a vs magnetic tilt θ_B, normalized to values at $\theta_B = 0$.

is common to refer to their dominant m and k_z components. One of the more prevalent asymmetries is a $m = 1$, $k_z = \pi/L_p$ "tilt" of the magnetic field with respect to the trap axis, characterized by an angle $\theta_B \equiv B_\perp/B_z$.

The qualitative behavior of the asymmetry mode remains unchanged even with moderately large magnetic tilt. Figure 7 shows f_a decreasing linearly by 30% and γ_a decreasing by 60% at fixed $V_{sq} = -10$ V as the magnetic tilt is increased to $\theta_B = \pm 3 \times 10^{-3}$ radian. These quantitative changes are mainly due to a decrease in the plasma potential ϕ_0 (caused by tilt-induced particle transport). Consequently, the ratio V_{sq}/ϕ_0 increases and the effective trapping barrier is enhanced. This will produce a decrease in the mode frequency and decay rate according to the trends depicted in Figs. 3 and 4.

Trapped particles may be an inherent part of Penning-Malmberg traps for a variety of reasons. Some intentional manipulations, such as "squeeze damping" of the diocotron mode [7, 8] obviously create equilibria as described here. The wide variety of "nested traps" being built for overlapping confinement of positrons and anti-protons [9, 10] have populations of trapped and untrapped particles. Most subtly, z-variations in the effective wall voltage can arise from small unintentional construction anomalies. For example, a variation in wall radius among cylinders gives an effective potential $V_{sq} \approx \phi_0 \, \Delta R_w/R_w$; this gives a trapped fraction $\varepsilon_{tr} \approx \Delta R_w/R_w$, so $\varepsilon_{tr} \gtrsim 10^{-3}$ is probably common to all devices.

The existence of trapped particle asymmetry modes substantially alters the theory perspective on particle transport due to θ-asymmetries in the trap construction. Resonant particle transport theories [3] utilize integration along unperturbed orbits, which is invalid with the bulk trapped particle populations described here, or even with microscopic trapping [11]. Similarly, 2D bounce-averaged invariants suggest that particles are confined to equipotential surfaces, and a k_z variation is required for radial particle transport; however, all previously-known modes with $k_z \neq 0$ have frequencies near ω_p, as opposed to f_d.

Experimentally, there are strong indications that the asymmetry mode contributes to
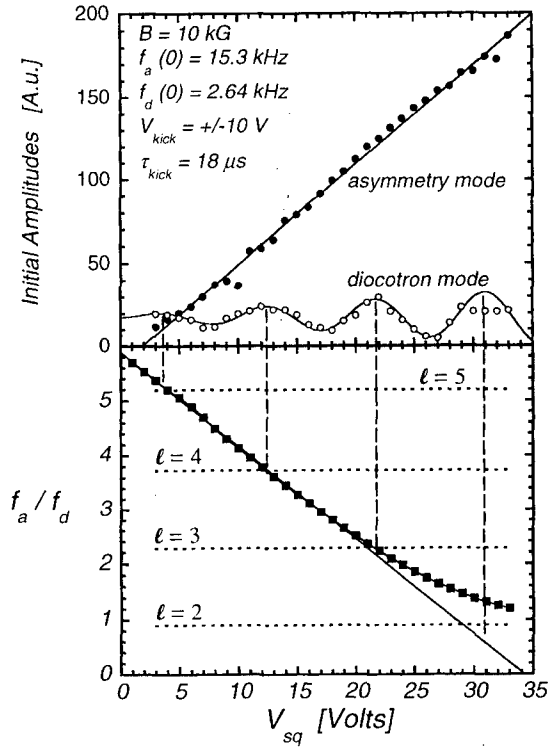
FIGURE 8. (a) "Excitability" of the asymmetry (closed circles) and diocotron (open circles) modes vs squeeze voltage V_{sq}. (b) Measured ratio f_a/f_d (squares) vs squeeze voltage V_{sq}. The horizontal dashed lines show the resonance [Eq. (6)] of sloshing particles. The vertical dashed line indicates an obvious correspondence of these resonances to the maxima in the diocotron mode amplitude.

asymmetry-induced transport by coupling between the static $m \neq 0$ $k_z \neq 0$ asymmetry and the $k_z \approx 0$ diocotron modes. When the external asymmetry is a magnetic tilt ($\theta_B \neq 0$), the diocotron mode has axially sloshing particles [12] at low frequency $f_d \ll f_b$, which can be thought of as a slow change in the equilibrium. A simple picture of what occurs with a misaligned plasma column is that the particles tend to accumulate wherever they can be closer along the magnetic field lines to their image charge in the wall, since that is a region of lower energy. Consequently, a small amount of the density ($\delta n \propto \theta_B$) sloshes axially from one end to the other as the diocotron mode causes the plasma column to orbit around the magnetic axis of the trap. This axial motion can then couple to the axially sloshing interior particles in the asymmetry mode. The coupling leads to the diocotron mode damping through excitation of the strongly damped asymmetry modes, and consequently to bulk radial transport of the particles.

The characteristics of this coupling are presently being investigated. Figure 8(a) shows the "excitability" of the asymmetry and diocotron modes as functions of the applied squeeze voltage. "Excitability" is simply the initial amplitude of the mode excited from

285

the wall sectors by a fixed $m = 1$ kick with odd parity in z (Fig. 1). The small excitation of the diocotron mode at $V_{sq} \approx 0$ occurs only because the sectors at $\pm z$ have slightly different coupling to the plasma. As squeeze voltage is increased, the asymmetry mode "excitability" increases linearly, in accord with the change of the trapped particle fraction ε_{tr}. In contrast, the excitation of the diocotron mode shows increasing oscillations about the $V_{sq} \approx 0$ level [Fig. 6(a)].

The maxima in these oscillations may be due to resonance in the axial velocities of sloshing particles shared by the two modes. Thus, we could expect that in resonance

$$
\frac{f_E - f_a}{2\pi k_a} = \frac{f_E - \ell f_d}{2\pi k_d},
$$
(5)

where k_a and k_d are effecctive axial wave vectors $(k_a > k_d)$ for the sloshing particles in corresponding modes, and $\ell = 2, 3 \dots$ is the order of the resonance. Figure 8(b) shows the measured ratio f_a/f_d as a function of the squeeze voltage. Comparing Figs. 8(a,b), we see that the maxima in the diocotron mode amplitude corresponds to the particular ratios of these mode frequencies, obtained directly from Eq. (5) using a quite reasonable ratio of the wave vectors $k_a/k_d \approx 1.45$ as the single adjustable parameter

$$
\frac{f_a}{f_d} = \ell \frac{k_a}{d_d} + \frac{f_E}{f_d} \left(1 - \frac{k_a}{k_d} \right) .
$$
(6)

This result may provide a clue as to why the diocotron mode has shown a squeeze dependent damping [7, 8]. Of course, the underlying assumptions and simplifications of the observed coupling remain to be examined. Nevertheless, our results allow us to speculate that the asymmetry modes are important in coupling trap asymmetries to particle motions and low frequency $\mathbf{E} \times \mathbf{B}$ drift modes.

ACKNOWLEDGMENTS

REFERENCES

1. J.J. Bollinger, R.L. Spencer, and R.C. Davidson (editors), *Non-Neutral Plasma Physics III*, American Institute of Physics Conf. Proc. 498 (New York: American Institute of Physics, 1999).
2. J.M. Kriesel and C.F. Driscoll, Phys. Rev. Lett. **85**, 2510 (2000).
3. D.L. Eggleston and T.M. O'Neil, Phys. Plasmas **6**, 2699 (1999).
4. A.J. Redd, *et al.*, Phys. Plasmas **6**, 1162 (1999).
5. M. Nadeem, *et al.*, Plasma Phys. Control. Fusion **37**, 1169 (1995).
6. K.S. Fine, W.G. Flynn, A.C. Cass, and C.F. Driscoll, Phys. Rev. Lett. **75**, 3277 (1995).
7. B.P. Cluggish, Ph.D. thesis, Univ. of California at San Diego (1995).
8. K.S. Fine, Ph.D. thesis, Univ. of California at San Diego (1989).
9. M. Charlton, *et al.*, Phys. Rep. **214** (2), 67 (1994).
10. D. Hall and G. Gabrielse, Phys. Rev. Lett. **77**, 1962 (1996).
11. D.H.E. Dubin, Phys. Rev. Lett. **79**, 2678 (1997).
12. G.W. Hart, Phys. Fluids B **3**, 2987 (1991).